JOURNAL OF GUIDANCE, CONTROL, AND DYNAMICS
Vol. 31, No. 4, July–August 2008

Analysis of Wing Rock Due to Rolling-Moment Hysteresis

Tiauw Hiong Go* and Fidelis Adhika Pradipta Lie†
Nanyang Technological University, Singapore 639798, Republic of Singapore

DOI: 10.2514/1.33216

This paper examines the single-degree-of-freedom wing-rock dynamic characteristics due to the presence of hysteresis in the static rolling-moment coefficient with respect to the sideslip angle. Two simplified hysteresis cases are considered: one represents full hysteresis and the other represents partial hysteresis. The approach used for analyzing the problem is analytical, using the multiple-time-scales method. Using such an approach, approximate solutions for the wing-rock amplitudes and frequencies as functions of the hysteresis parameters are obtained. These analytical solutions, which lead to considerable insight into the aerodynamic hysteresis effect on wing rock, are demonstrated to be in good agreement with the numerical results. It is also shown that, unlike the case involving the nonhysteretic type of nonlinearity, in the presence of the hysteresis, wing rock can occur before the loss of the dynamic roll-damping derivative.

Nomenclature

A	=	amplitude of oscillation
A_∞	=	steady-state amplitude
B	=	phase correction
b	=	wing span
C_l	=	rolling-moment coefficient
$\tilde{d}$	=	εd, hysteresis height parameter
$\tilde{h}(\beta, \dot{\beta})$	=	hysteresis function
I_{xx}	=	moment of inertia about the roll axis
L	=	rolling moment
$\mathcal{O}(.)$	=	order-of-magnitude notation
p	=	roll rate
q	=	dynamic pressure
S	=	wing area
t	=	time
W	=	work
α	=	angle of attack
β	=	angle of sideslip
δ	=	$\Phi_2 - \Phi_1$, hysteresis transition width
ε	=	small parameter
$\tilde{\mu}$	=	$\varepsilon\mu$, roll-damping parameter
τ_i	=	time scales
Φ	=	hysteresis width parameter
Φ_i	=	hysteresis transition roll angle
ϕ	=	roll angle
ω	=	natural frequency of motion
$\wedge$	=	logical and
$\vee$	=	logical or
$(\dot{\cdot})$	=	$\mathrm{d}/\mathrm{d}t$, differential with respect to time

I. Introduction

WING rock is uncommanded roll-dominated oscillatory motion that an aircraft can experience in flight at high angles of attack. Wing rock is a nonlinear phenomenon, manifested as limit cycles [1–8], that could severely limit the maneuver performance of an aircraft and could even lead to catastrophic consequences. The degree of severity of wing rock is determined mainly by the amplitude of the limit cycles and, to a lesser extent, by its frequency.

Mathematically, wing rock can occur when one or more nonlinear terms are present in the equation(s) of motion. Possible scenarios leading to the occurrence of wing rock are the variation of damping in roll with angle of sideslip, cubic variation of lateral derivatives with roll rate and sideslip, and the presence of aerodynamic hysteresis in the static rolling moment [9]. The first two scenarios have been extensively studied [1–8]. Single- [1,3–5] and multiple-degree-of-freedom cases [2,6–8] involving these scenarios have been examined. In such scenarios, wing-rock occurrence is primarily associated with the loss of dynamic roll or lateral–directional damping derivative at high angles of attack. The latter is for the case involving both roll and yaw degrees of freedom.

Some examples of hysteresis in the lateral aerodynamic coefficients with angle of sideslip are shown in Fig. 1 [9]. Other experimental results on rolling-moment hysteresis can also be seen in [10]. In contrast with the first two preceding scenarios, only a few works have been reported on the investigation of wing rock due to aerodynamic hysteresis, for example [11,12]. Such hysteresis, which could be due to asymmetric vortex shedding, vortex breakdown, or periodic flow separation and reattachment, is characterized by a double-valued behavior of the steady-state aerodynamic response to variations in one of the motion variables such as angle of attack, angle of sideslip, or spin rate [9]. Schmidt [11] used a control theory approach to demonstrate the occurrence of wing rock in the presence of a simple hysteresis in the variation of rolling-moment coefficient with respect to sideslip. Schiff and Tobak [12] used an aerodynamic mathematical formulation that allows for hysteresis to explain the seemingly anomalous data observed from some wind-tunnel wing-rock measurements. Using such formulation, they were able to explain the effects of the hysteresis on the effective dynamic roll-damping coefficient.

This paper is intended to further the work in the area by addressing the detailed interrelation of the static rolling-moment hysteresis parameters with the wing-rock properties, which has not been covered in the previous works. In this attempt, only a single degree of freedom in roll is considered. Simple hysteresis models, such as those used in [11,12], are used in the analysis. The approach used in the study here is analytical, employing the multiple-time-scale (MTS) method. This method has been used by Elzebda et al. [4] and Nayfeh et al. [5] to study the effect of the cubic variation of the rolling-moment derivatives with respect to the angle of attack on the single-degree-of-freedom wing-rock motion. Go and Ramnath [6–8] also used this method, in conjunction with the center manifold and bifurcation analysis, to solve for the multiple-degree-of-freedom wing-rock cases. As can be seen later, by using the MTS method, approximate solutions of the problem in parametric form can be obtained. This approach seems to offer considerable advantages over

Received 19 July 2007; revision received 11 December 2007; accepted for publication 11 December 2007.

*Assistant Professor, School of Mechanical and Aerospace Engineering. Member AIAA.

†Research Student, School of Mechanical and Aerospace Engineering. Student Member AIAA.

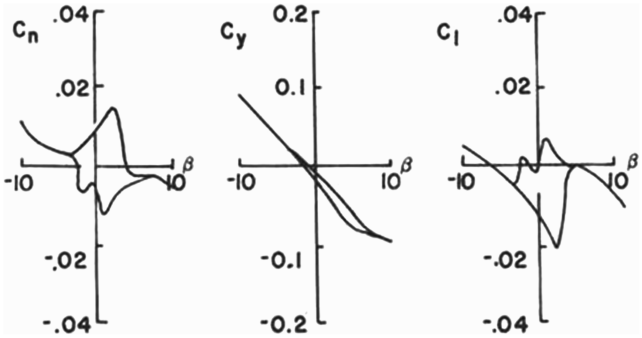

Fig. 1 Moment and force coefficient hysteresis with angle of sideslip [9].

numerical methods because the parameter interdependence can be explicitly seen.

II. Equation of Motion

The equation of motion for the single-degree-of-freedom aircraft's roll motion at specific altitude, velocity, and angle of attack can be expressed as follows:

$$I_{xx}\ddot{\phi} = L(p, \beta, \dot{\beta}) \tag{1}$$

where I_{xx} is the moment of inertia of the aircraft about the roll axis; $\ddot{\phi}$ is the second time derivative of the roll angle ϕ; and L is the aerodynamic rolling moment, which, in general, is a function of roll rate p, angle of sideslip β, and sideslip rate $\dot{\beta}$. Because the purpose of the study is to investigate the effects of the hysteresis parameters on the resulting motion, only the hysteretic type of nonlinearity is considered in L, and the other terms are assumed to be linear. Consequently, the rolling moment can be expressed as

$$L = L_p p + L_\beta \beta + L_{\dot{\beta}}\dot{\beta} + \tilde{h}(\beta, \dot{\beta}) \tag{2}$$

where L_p, L_β, and $L_{\dot{\beta}}$ are the rolling-moment derivatives with respect to the roll rate, sideslip angle (often called *effective dihedral*), and sideslip rate, respectively; $h(\beta, \dot{\beta})$ denotes the static rolling-moment hysteretic nonlinearity, the form of which depends on the hysteresis model considered; and the combination of the terms $L_\beta \beta + \tilde{h}(\beta, \dot{\beta})$ represents the static rolling moment of the system.

For an aircraft with only a roll degree of freedom,

$$p = \dot{\phi}, \qquad \beta = \phi \sin\alpha, \qquad \dot{\beta} = \dot{\phi}\sin\alpha \tag{3}$$

where α is the angle of attack. Through these kinematic relations, all functional relationships involving β or $\dot{\beta}$ can be represented as a functional relationship with ϕ or $\dot{\phi}$. The substitution of Eqs. (2) and (3) into Eq. (1) yields

$$\ddot{\phi} + \omega^2\phi = \tilde{\mu}\,\dot{\phi} + \tilde{h}(\phi, \dot{\phi}) \tag{4}$$

where

$$\omega^2 = -\frac{L_\beta \sin\alpha}{I_{xx}}$$

and

$$\tilde{\mu} = \frac{L_p + L_{\dot{\beta}}\sin\alpha}{I_{xx}}$$

represent the linear stiffness coefficient (contributed mainly by effective dihedral) and dynamic roll-damping derivative, respectively. Equation (4) is the general equation of rolling motion involving hysteretic nonlinearity and is the focus of the analysis here. At high angles of attack and in the vicinity of wing rock, the damping coefficient is usually small. Then, by considering the case in which the hysteretic nonlinearity is also small (i.e., small $|\tilde{h}(\phi, \dot{\phi})|$), which physically corresponds to the situation in which hysteresis starts to appear in the system, Eq. (4) can be parameterized as follows:

$$\ddot{\phi} + \omega^2\phi = \varepsilon(\mu\dot{\phi} + h(\phi, \dot{\phi})) \tag{5}$$

where $\tilde{h}(\phi, \dot{\phi}) = \varepsilon h(\phi, \dot{\phi})$ and $\tilde{\mu} = \varepsilon\mu$ with $|\varepsilon| \ll 1$. Equation (5) is in the form that is suitable for the application of the MTS method, as described next. Note that in general, the results obtained using the MTS approach are only valid when the preceding assumptions leading to the parameterization in Eq. (5) are satisfied.

III. MTS Method

The MTS method [13,14] is an analytical approach to obtain approximate solutions to physical problems involving a mixture of rapid and slow variations. A problem of this kind is usually recognized by the existence of a small parameter in its formulation. The main idea of the MTS approach is the selection of the appropriate *time scales* to observe the behavior of a system. The number of time scales chosen may affect the level of accuracy of the solution obtained. In many applications, however, the use of only two time scales is often adequate to capture the important aspects of the system dynamics.

In the mechanization of the MTS method, the independent variable, which is time t in this context, is extended to a space of higher dimension:

$$t \to \{\tau_0, \tau_1, \ldots, \tau_n\} \tag{6}$$

The *time scales* $\tau_0, \tau_1, \ldots, \tau_n$, which are normally functions of t and the small parameter ε [i.e., $\tau_i = f_i(t, \varepsilon)$; $|\varepsilon| \ll 1$], are the result of this extension. Each time scale captures a certain behavior of the system. The relation between τ_i and ε in this case determines whether the time scale is fast or slow. Figure 2 illustrates this concept.

For an ordinary differential equation, as the consequence of the extension of t, the dependent variable $y(t, \varepsilon)$ is also extended as

$$y(t, \varepsilon) \to Y(\tau_0, \tau_1, \ldots, \tau_n, \varepsilon) \tag{7}$$

Therefore, an ordinary differential equation will become a partial differential equation. The resulting partial differential equation, however, is often simpler and easier to solve than the initial ordinary differential equation. Once Y is solved, one can substitute back the time scales to get the approximate solution in time t:

$$Y(\tau_0(t, \varepsilon), \tau_1(t, \varepsilon), \ldots, \tau_n(t, \varepsilon), \varepsilon) = y(t, \varepsilon) \tag{8}$$

For the equation of motion (5), the MTS method is invoked with the following extensions:

$$t \to \{\tau_0, \tau_1\} \qquad \tau_0 = t, \qquad \tau_1 = \varepsilon t \tag{9}$$

$$\phi(t) \to \phi_0(\tau_0, \tau_1) + \varepsilon\phi_1(\tau_0, \tau_1) + \mathcal{O}(\varepsilon^2) \tag{10}$$

In this formulation, τ_0 and τ_1 represent the fast and the slow time scales, respectively. With this extension, Eq. (5) becomes

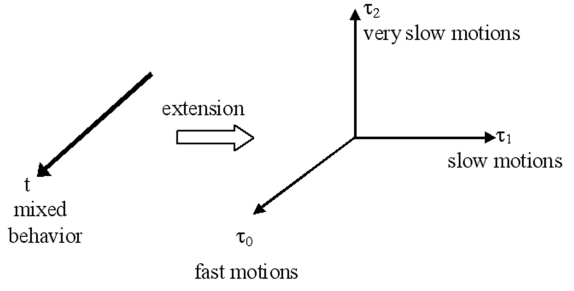

Fig. 2 The concept of extension [13,14].

$$\frac{\partial^2\phi_0}{\partial\tau_0^2}+\omega^2\phi_0+\varepsilon\left(\frac{\partial^2\phi_1}{\partial\tau_0^2}+2\frac{\partial^2\phi_0}{\partial\tau_0\partial\tau_1}+\omega_0^2\phi_1\right)$$
$$=\varepsilon\left(\mu\frac{\partial\phi_0}{\partial\tau_0}+h(\phi_0,\dot{\phi}_0)\right)+\mathcal{O}(\varepsilon^2) \tag{11}$$

Only terms up to $\mathcal{O}(\varepsilon)$ are retained in the preceding equation, because these are sufficient to obtain the zeroth-order approximation of the solution. Equating groups of the same order on the left- and the right-hand sides of Eq. (11) leads to

$\mathcal{O}(1)$:

$$\frac{\partial^2\phi_0}{\partial\tau_0^2}+\omega^2\phi_0=0 \tag{12}$$

$\mathcal{O}(\varepsilon)$:

$$\frac{\partial^2\phi_1}{\partial\tau_0^2}+2\frac{\partial^2\phi_0}{\partial\tau_0\partial\tau_1}+\omega^2\phi_1=\mu\frac{\partial\phi_0}{\partial\tau_0}+h\left(\phi_0,\frac{\partial\phi_0}{\partial\tau_0}\right) \tag{13}$$

The $\mathcal{O}(1)$ equation does not depend on $h(\phi,\dot{\phi})$; thus, regardless of the hysteresis model used, the zeroth-order solution will have the following form:

$$\phi_0=A(\tau_1)\sin\psi,\qquad \psi\equiv\omega\tau_0+B(\tau_1) \tag{14}$$

This means that the resulting motion is oscillatory. The functions A and B represent the amplitude and the phase correction of the solution. Note that, in general, A and B vary with the slow time scale τ_1. Once these variations are known, the zeroth-order approximation of the motion dynamics is complete. These variations are found by substituting Eq. (14) into Eq. (13), which yields

$$\frac{\partial^2\phi_1}{\partial\tau_0^2}+\omega^2\phi_1=\left(\mu A\omega-2\frac{\mathrm{d}A}{\mathrm{d}\tau_1}\omega\right)\cos\psi$$
$$+\left(2A\omega\frac{\mathrm{d}B}{\mathrm{d}\tau_1}\right)\sin\psi+h\left(\phi_0,\frac{\partial\phi_0}{\partial\tau_0}\right) \tag{15}$$

Equation (15) suggests that the amplitude and phase properties depend on the rolling-moment hysteresis involved. Evaluation of these properties for two types of hysteresis is discussed next.

IV. Case I: Full Hysteresis of C_l vs β

This form of hysteresis is the same as that used by Schmidt [11]. In this case, the rolling-moment coefficient C_l is double-valued for all values of β (or, equivalently, ϕ), as depicted in Fig. 3. The value of C_l depends on the sign of the sign of $\dot{\beta}$ (or $\dot{\phi}$). As the arrows indicate, when $\dot{\beta}$ is positive, it follows the upper path, and when $\dot{\beta}$ is negative, it follows the lower path. These upper and lower paths are assumed to be parallel and have equal-but-opposing sign crossing values with respect to the vertical axis ($\pm\Delta C_l$). In this case, the hysteresis loop is of the form of a parallelogram of height $2\Delta C_l$. The jumps between these two paths are assumed to be perfectly vertical, which indicates the instantaneous change of values when $\dot{\beta}$ changes sign.

Mathematically, the contribution of this hysteresis to the rolling-moment coefficient can be expressed as

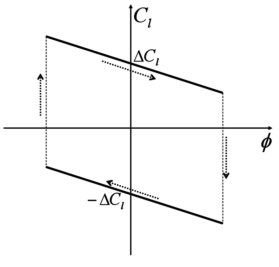

Fig. 3 Static rolling-moment full-hysteresis curve.

$$C_{l,\text{hysteresis}}=\Delta C_l\,\mathrm{sgn}(\dot{\phi}) \tag{16}$$

For this hysteresis, $\tilde{h}(\phi,\dot{\phi})$ in Eq. (4) can be written as

$$\tilde{h}(\dot{\phi})=\tilde{d}\,\mathrm{sgn}(\dot{\phi}) \tag{17}$$

where $\tilde{d}\equiv\Delta C_l qSb/I_{xx}$. Note that q is the dynamic pressure, S is the wing area, and b is the wing span. In this case, $\tilde{h}$ is a function of $\dot{\phi}$ only, and with ε parameterization, as in Eq. (5), one gets

$$h(\dot{\phi})=d\,\mathrm{sgn}(\dot{\phi}) \tag{18}$$

where $\tilde{d}=\varepsilon d$.

To find the amplitude and phase variations due to such hysteresis, Eq. (18) is substituted into Eq. (15) to yield

$$\frac{\partial^2\phi_1}{\partial\tau_0^2}+\omega^2\phi_1=\left(\mu A\omega-2\frac{\mathrm{d}A}{\mathrm{d}\tau_1}\omega\right)\cos\psi$$
$$+\left(2A\omega\frac{\mathrm{d}B}{\mathrm{d}\tau_1}\right)\sin\psi+d\,\mathrm{sgn}(\cos\psi) \tag{19}$$

To get a continuous and smooth mathematical representation, the last nonlinear term is expanded by using the Fourier series [15], as follows:

$$\mathrm{sgn}\,(\cos\psi)=\frac{4}{\pi}\cos\psi-\frac{4}{3\pi}\cos 3\psi+\cdots \tag{20}$$

By retaining only the first harmonic term of the expansion, Eq. (19) becomes

$$\frac{\partial^2\phi_1}{\partial\tau_0^2}+\omega^2\phi_1=\left(\mu A\omega-2\frac{\mathrm{d}A}{\mathrm{d}\tau_1}\omega+\frac{4d}{\pi}\right)\cos\psi$$
$$+\left(2A\omega\frac{\mathrm{d}B}{\mathrm{d}\tau_1}\right)\sin\psi \tag{21}$$

Nonzero $\cos\psi$ and $\sin\psi$ terms on the right-hand side of the equation give rise to secular terms of the form $\tau_0\cos\psi$ and $\tau_0\sin\psi$ in the solution for ϕ_1. Such secular terms make the solution nonuniform, because $\tau_0\cos\psi$ and $\tau_0\sin\psi\to\infty$ as $\tau_0\to\infty$. Therefore, to obtain a uniform solution, the coefficients of the $\cos\psi$ and $\sin\psi$ terms must be set to zero. This leads to the following amplitude and phase-correction equations:

$$\frac{\mathrm{d}A}{\mathrm{d}\tau_1}=\frac{\mu}{2}A+\frac{2d}{\pi\omega} \tag{22}$$

$$\frac{\mathrm{d}B}{\mathrm{d}\tau_1}=0 \tag{23}$$

The solution of the phase-correction equation (23) yields

$$B=\text{constant} \tag{24}$$

This means that the wing-rock frequency is constant and is the same as ω. In other words, the wing-rock frequency is proportional to the square root of the aircraft's effective dihedral.

Integration of the amplitude Eq. (22) results in

$$A=-\frac{4d}{\pi\mu\omega}+\left(K+\frac{4d}{\pi\mu\omega}\right)\exp\left(\frac{\mu\tau_1}{2}\right) \tag{25}$$

where K is a constant of integration determined by the initial condition.

If $\mu>0$, the amplitude of the oscillations diverges. If $\mu<0$, the second term in the right-hand side of Eq. (24) decays exponentially in τ_1 and as $\tau_1\to\infty$, this term goes to zero. In other words, the amplitude becomes constant in the steady-state condition. This is the situation in which sustained limit-cycle oscillations (wing rock) occur. The steady-state wing-rock amplitude is given by

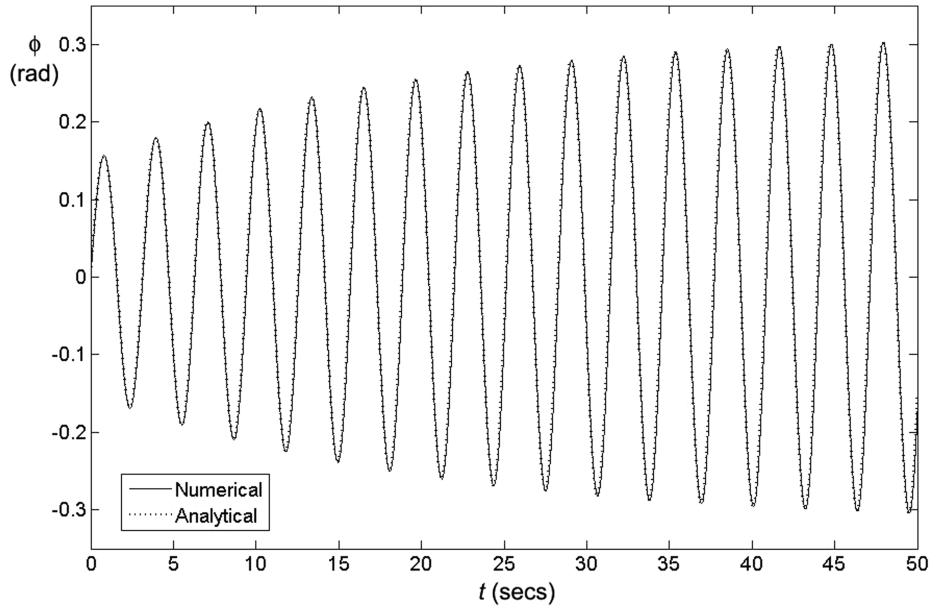

Fig. 4 Wing rock for $C_l - \beta$ full hysteresis; $\omega = 2$ rad/s^2, $\tilde{\mu} = -0.1$ s^{-1}, and $\tilde{d} = 0.05$ s^{-2}, with initial condition $(\phi, \dot{\phi}) = (0, 0.3$ rad/s).

$$A_\infty = -\frac{4\tilde{d}}{\pi\tilde{\mu}\omega} \tag{26}$$

This result suggests that the amplitude of the steady-state wing-rock motion is proportional to the hysteresis height (ΔC_l through $\tilde{d}$) and inversely proportional to the dynamic roll-damping derivative $\tilde{\mu}$ and to the frequency of the motion ω.

The condition for the sustained wing rock in the presence of the static rolling-moment full hysteresis is different from that with the nonhysteretic type of nonlinearities, as presented in [1–8]. With the nonhysteretic nonlinearities, wing rock is developed due to the loss of the dynamic roll-damping derivative ($\tilde{\mu} \geq 0$). However, in the presence of the hysteresis, sustained wing rock occurs when the dynamic roll damping is still present ($\tilde{\mu} < 0$). In this case, the onset of wing rock is the onset of the hysteresis itself.

The accuracy of this analytical approach is examined by comparing the results with those obtained from direct numerical integration of Eq. (4), with $\tilde{h}$ as given by Eq. (17). The values of the parameters ω and $\propto$ are chosen to be within the range of typical values for small fighter aircraft at high angles of attack. Figure 4 shows such a comparison for $\omega = 2$ rad/s^2, $\tilde{\mu} = -0.1$ s^{-1}, and $\tilde{d} = 0.05$ s^{-2} with the same initial conditions. In this case, the analytical approximation is in excellent agreement with the numerical integration result. The transient and steady-state wing-rock motions are predicted very accurately by the analytical solution. Table 1 presents comparison results for other parameters values. It can be observed from this table that for all the cases tried, excellent agreement (up to three decimal digits) between the analytical and numerical results is demonstrated.

Table 1 Comparison between numerical and analytical results for full $C_l - \beta$ hysteresis

ω, rad/s	$-\tilde{\mu}$, s^{-1}	$\tilde{d}$, s^{-2}	Numerical amplitude, rad	Analytical amplitude, rad
1.50	0.10	0.03	0.2547	0.2546
1.50	0.10	0.05	0.4245	0.4244
1.50	0.20	0.03	0.1275	0.1273
1.50	0.20	0.05	0.2124	0.2122
2.00	0.10	0.03	0.1907	0.1910
2.00	0.10	0.05	0.3184	0.3183
2.00	0.20	0.03	0.0956	0.0955
2.00	0.20	0.05	0.1592	0.1592

V. Case II: Partial Hysteresis of C_l vs β

A still-simplified, but more generic, hysteretic nonlinearity, similar to that formulated in [12], is considered here (see Fig. 5). In this case, C_l hysteresis does not occur for all values of β (or ϕ), but only within a certain range ($-\Phi \leq \phi \leq \Phi$). Within this range, C_l is double-valued depending upon the sign of $\dot{\beta}$ (or $\dot{\phi}$), as indicated by the arrows in Fig. 5. For simplicity, the hysteresis paths are assumed to be parallel and the jumps are perfectly vertical. With these assumptions, the hysteresis loop forms a parallelogram of height $2\Delta C_l$ and width 2Φ.

Such hysteresis can be expressed as

$$h(\phi, \dot{\phi}) = \begin{cases} d; & \phi \leq -\Phi \\ d\,\mathrm{sgn}(\dot{\phi}); & -\Phi < \phi < \Phi \\ -d; & \phi \geq \Phi \end{cases} \tag{27}$$

where d is defined as before. As in the previous case, h is substituted into Eq. (15) and then $h(\phi_0, (\partial\phi_0/\partial\tau_0))$ is approximated using Fourier series expansion, as follows [15]:

$$h = \frac{4d}{\pi}\left(\frac{\Phi}{A}\cos\psi - \sqrt{1 - \left(\frac{\Phi}{A}\right)^2}\sin\psi\right) + \cdots \tag{28}$$

Equation (28) only shows the first harmonic terms of the expansion, which is sufficient to obtain the zeroth-order approximation of the solution. Substituting Eq. (28) into Eq. (15) gives

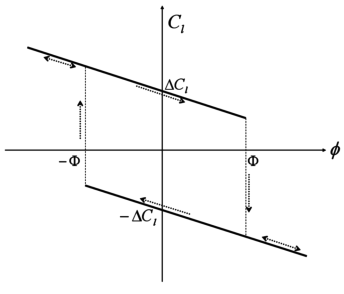

Fig. 5 Static rolling-moment partial-hysteresis curve.

$$\frac{\partial^2\phi_1}{\partial\tau_0^2}+\omega^2\phi_1=\left(\mu A\omega-2\frac{\mathrm{d}A}{\mathrm{d}\tau_1}\omega+\frac{4d\Phi}{\pi A}\right)\cos\psi + \left(2A\omega\frac{\mathrm{d}B}{\mathrm{d}\tau_1}-\frac{4d}{\pi}\sqrt{1-\left(\frac{\Phi}{A}\right)^2}\right)\sin\psi \tag{29}$$

Setting the coefficients of the $\cos\psi$ and $\sin\psi$ terms to zero to avoid the secular terms leads to the following amplitude and phase-correction equations:

$$\frac{\mathrm{d}A}{\mathrm{d}\tau_1}=\frac{\mu}{2}A+\frac{2d\Phi}{\pi\omega A} \tag{30}$$

$$\frac{\mathrm{d}B}{\mathrm{d}\tau_1}=\frac{2d}{\pi\omega A}\sqrt{1-\left(\frac{\Phi}{A}\right)^2} \tag{31}$$

Solving Eq. (30) by means of separation of variables and integration yields

$$A=\sqrt{-\frac{4\tilde{d}\Phi}{\tilde{\mu}\pi\omega}+k\exp(\mu\tau_1)} \tag{32}$$

where k is a constant of integration, the value of which depends on the initial condition. It can be observed from Eq. (32) that sustained wing rock occurs when $\mu<0$, because the second term under the square root sign decays to zero as $\tau_1\to\infty$. The amplitude of the steady wing-rock motion is

$$A_\infty=\sqrt{-\frac{4\tilde{d}\Phi}{\tilde{\mu}\pi\omega}} \tag{33}$$

Note that $4\tilde{d}\Phi\propto 4\Delta C_l\Phi$, which is the area of the hysteresis loop. Hence, this result suggests that for the type of the hysteresis pattern considered, the wing-rock amplitude is proportional to the square root of the area of hysteresis loop. This statement is also valid for the full-hysteresis case (case I) by replacing Φ in Eq. (33) with A_∞. This makes sense from the energy point of view, because hysteresis area is proportional to the energy pumped into the system. The larger the hysteresis area, the larger the energy that is pumped into the system, and, consequently, the larger the resulting wing-rock amplitude.

Equation (31) can be solved by integration once the expression for the amplitude is obtained. This leads to

Table 2 Comparison between the analytical and numerical results for $C_l-\beta$ partial hysteresis for various values of Φ ($\omega=2$ rad/s^2, $\tilde{\mu}=-0.1$ s^{-1}, and $\tilde{d}=0.05$ s^{-2})

Φ, rad	Analytical		Numerical	
	Amplitude, rad	Period, s	Amplitude, rad	Period, s
0.100	0.1784	3.0300	0.1751	3.0367
0.175	0.2360	3.0721	0.2338	3.0750
0.200	0.2523	3.0825	0.2504	3.0825
0.225	0.2676	3.0900	0.2661	3.0900
0.250	0.2821	3.1000	0.2809	3.0967
0.275	0.2959	3.1100	0.2950	3.1125
0.300	0.3090	3.1200	0.3086	3.1225

$$B(\tau_1)=\int\frac{2d}{\pi A\omega}\sqrt{1-\left(\frac{\Phi}{A}\right)^2}\,\mathrm{d}\tau_1+B_0 \tag{34}$$

where B_0 is a constant of integration that is determined from the initial condition. Note that for Eq. (34) to be real, the following condition must be satisfied:

$$\Phi<-\frac{4\tilde{d}}{\tilde{\mu}\pi\omega} \tag{35}$$

The situation in which this is not satisfied corresponds to the oscillation that occurs only within the hysteresis region, which leads back to case I.

Figure 6 compares the numerical and the analytical results for $\omega=2$ rad$\cdot$s^{-2}, $\tilde{\mu}=-0.1$ s^{-1}, $\tilde{d}=0.05$ s^{-2}, and $\Phi=0.1$ rad with the same initial conditions. Again, it can be observed that they are in very good agreement with each other. Table 2 shows the comparison between the numerical and analytical result for various values of Φ. For the cases tried, agreement up to two decimal digits can be achieved.

VI. Deviations to Partial-Hysteresis Case

Some deviations to the ideal case-II hysteresis type are also studied to examine the generalizability of the results obtained. The deviations considered are shown in Figs. 7 and 8. The first type of deviation (Fig. 7) accommodates the case in which the jumps are not vertical, but are still parallel to each other. The second type of deviation (Fig. 8) exemplifies the case in which the $C_l-\phi$ gradient on the hysteresis loop is different from that outside of the loop. Analyses for these two types of deviations are presented next.

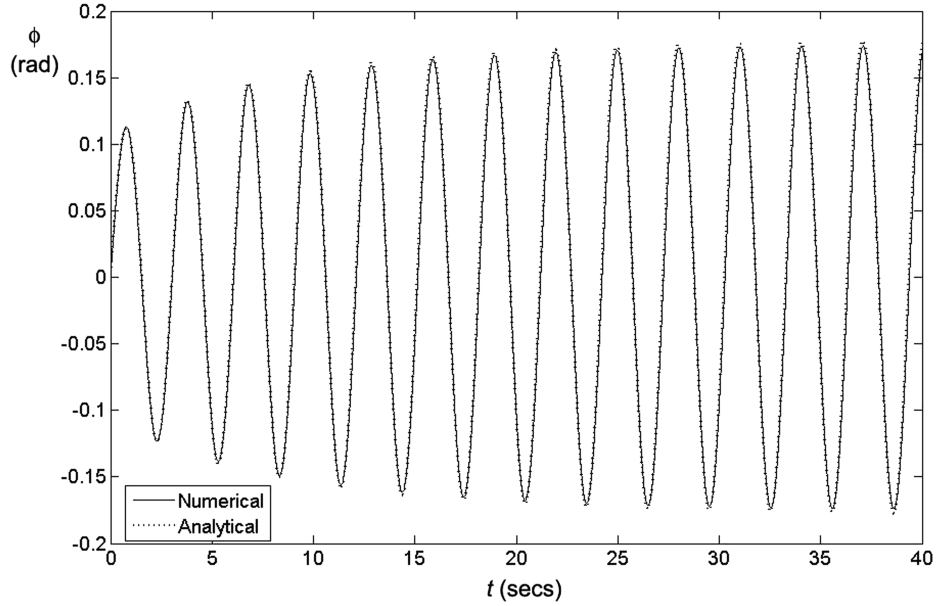

Fig. 6 Wing rock for $C_l-\beta$ partial hysteresis; $\omega=2$ rad/s^2, $\tilde{\mu}=-0.1$ s^{-1}, $\tilde{d}=0.05$ s^{-2}, and $\Phi=0.1$ rad, with initial condition $(\phi,\dot{\phi})=(0, 0.2$ rad/s).

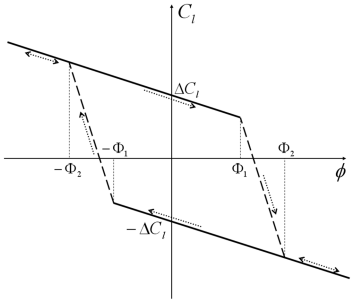

Fig. 7 Static rolling-moment hysteresis with nonvertical jumps; $\Phi_2 - \Phi_1 = \delta$ and $(\Phi_2 + \Phi_1)/2 = \Phi$.

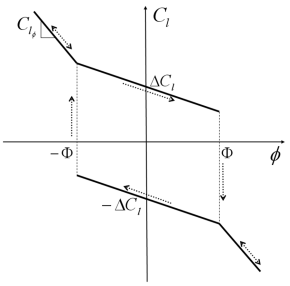

Fig. 8 Static rolling-moment coefficient with hysteresis gradient deviation.

By invoking the MTS method and expanding $h(\phi_0, (\partial\phi_0/\partial\tau_0))$ in terms of Fourier series, it can be shown that the steady wing-rock motion amplitude is still given by Eq. (33). However, the phase correction is now given by

$$B(\tau_1) = -\int \frac{p}{2A\omega}\,\mathrm{d}\tau_1 + B_0 \tag{37}$$

where

$$\begin{aligned} p = {} & \frac{2d}{\pi}\left(\frac{2\Phi}{\delta} - 1\right)\cos\left(\sin^{-1}\left(\frac{\Phi_1}{A}\right)\right) \\ & - \frac{2d}{\pi}\left(\frac{2\Phi}{\delta} + 1\right)\cos\left(\sin^{-1}\left(\frac{\Phi_2}{A}\right)\right) - \frac{2dA}{\delta\pi}\left(\sin^{-1}\left(\frac{\Phi_2}{A}\right)\right. \\ & \left. - \sin^{-1}\left(\frac{\Phi_1}{A}\right)\right) + \frac{dA}{\pi\delta}\left(\sin\left(2\sin^{-1}\left(\frac{\Phi_2}{A}\right)\right)\right. \\ & \left. - \sin\left(2\sin^{-1}\left(\frac{\Phi_1}{A}\right)\right)\right) \end{aligned} \tag{38}$$

Figure 9 shows the comparison between the analytical and numerical solutions for $\omega = 2$ rad $\cdot$ s^{-2}, $\tilde{\mu} = -0.1$ s^{-1}, $\tilde{d} = 0.1$ s^{-2}, $\Phi = 0.05$ rad, and $\delta = 0.02$ rad. This figure shows that the frequency predicted by the analytical method is in a good agreement with the numerical integration result. There are some discrepancies in the amplitude results; however, they are relatively small, which is less than 5% for this particular example. Table 3 shows further

A. Nonvertical Jump Deviation

For this deviation, $h(\phi, \dot{\phi})$ in Eq. (5) becomes

$$h(\phi,\dot{\phi}) = \begin{cases} d, & \phi < -\Phi_2 \\ -\frac{2d}{\delta}[\phi - \mathrm{sgn}(\dot{\phi})\Phi], & [(\dot{\phi} \geq 0) \wedge (\Phi_1 \leq \phi \leq \Phi_2)] \vee [(\dot{\phi} < 0) \wedge (-\Phi_2 \leq \phi \leq -\Phi_1)] \\ d\,\mathrm{sgn}(\dot{\phi}), & (-\Phi_2 \leq \phi \leq \Phi_1) \vee (-\Phi_1 \leq \phi \leq \Phi_2) \\ -d, & \phi > \Phi_2 \end{cases} \tag{36}$$

where d is as defined previously.

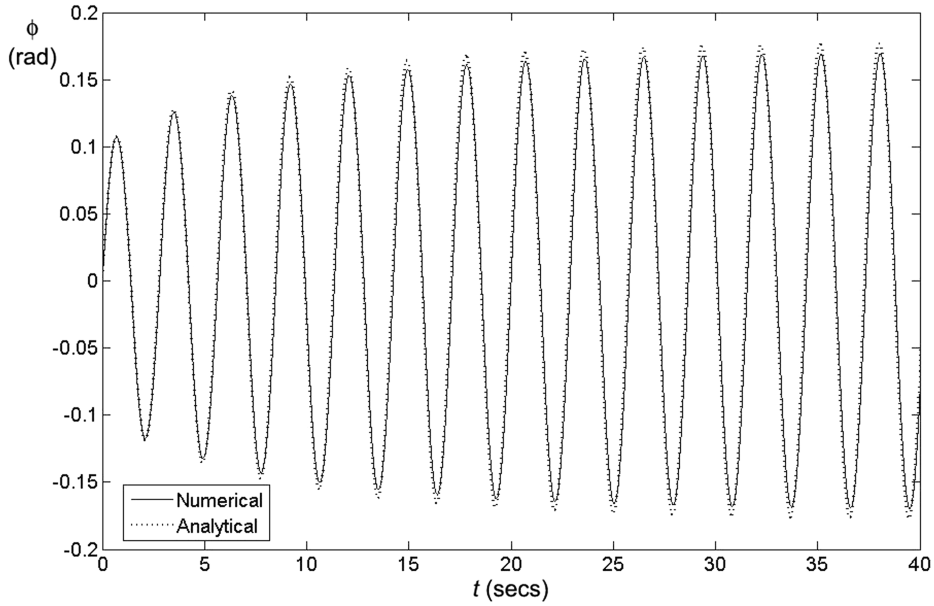

Fig. 9 Wing rock for $C_l - \beta$ hysteresis with nonvertical jumps; $\omega = 2$ rad $\cdot$ s^{-2}, $\tilde{\mu} = -0.1$ s^{-1}, $\tilde{d} = 0.1$ s^{-2}, $\Phi = 0.05$ rad, and $\delta = 0.02$ rad, with initial condition $(\phi, \dot{\phi}) = (0, 0.23$ rad/s).

Table 3 Comparison between the analytical and numerical results for nonvertical $C_l - \beta$ hysteresis ($\omega = 2$ rad $\cdot$ s^{-2}, $\tilde{\mu} = -0.1$ s^{-1}, $\tilde{d} = 0.1$ s^{-2}, and $\Phi = 0.05$ rad)

δ	Analytical		Numerical	
	Amplitude, rad	Period, s	Amplitude, rad	Period, s
0.01	0.1784	2.89	0.1705	2.89
0.02	0.1784	2.89	0.1705	2.90
0.03	0.1784	2.89	0.1705	2.90
0.04	0.1784	2.89	0.1705	2.90
0.05	0.1784	2.89	0.1705	2.90
0.06	0.1784	2.89	0.1705	2.90

Table 4 Comparison between the analytical and numerical results for $C_l - \beta$ hysteresis with gradient deviation ($\omega = 2$ rad $\cdot$ s^{-2}, $\tilde{\mu} = -0.1$ s^{-1}, and $\tilde{d} = 0.1$ s^{-2})

Φ, rad	Analytical		Numerical	
	Amplitude, rad	Period, s	Amplitude, rad	Period, s
0.05	0.1784	3.1491	0.1787	3.10
0.15	0.3090	3.1554	0.3100	3.15
0.25	0.3989	3.1606	0.4009	3.20
0.35	0.4720	3.1659	0.4751	3.15
0.45	0.5352	3.1721	0.5392	3.20
0.55	0.5917	3.1807	0.5968	3.20

comparison for various values of δ, while keeping ω, $\tilde{\mu}$, $\tilde{d}$, and Φ constant at the preceding values. As can be seen from this table, the changes in δ value virtually have no effect on the amplitude and frequency of wing rock, and the analytical results correctly predict this.

B. Hysteresis Gradient Deviation

For this type of deviation (Fig. 8), $h(\phi, \dot{\phi})$ can be expressed as follows:

$$h(\phi, \dot{\phi}) = [u(\phi + \Phi) - u(\phi - \Phi)]\left(d\,\mathrm{sgn}(\dot{\phi}) + \frac{d}{\Phi}\phi\right) \tag{39}$$

where u is the Heaviside or unit step function, and d is the hysteresis height parameter, as defined previously. Note that in the preceding equation, d/Φ indicates the gradient deviation of the hysteresis loop (compared with the gradient of the line outside of the hysteresis loop).

By using the same mathematical procedure as before, it can be shown that this deviation leads to the same steady-state wing-rock amplitude [Eq. (33)] and the same form of phase-correction equation (37) with

$$p = \left(\frac{2d}{\pi\Phi}\sin^{-1}\left[\frac{\Phi}{A}\right] - \frac{2d}{\pi A}\sqrt{1 - \left(\frac{\Phi}{A}\right)^2}\right)A \tag{40}$$

Figure 10 shows the comparison between the analytical and numerical solutions for $\omega = 2$ rad $\cdot$ s^{-2}, $\tilde{\mu} = -0.1$ s^{-1}, $\tilde{d} = 0.1$ s^{-2}, and $\Phi = 0.05$ rad. Again, this comparison indicates that the analytical results are fairly accurate. Moreover, Table 4 shows that the analytical prediction can hold up well against the numerical results for various values of Φ. Unlike the nonvertical jump deviation, the hysteresis gradient deviation can have significant effects toward the resulting wing-rock amplitudes. Wing-rock frequency is not affected much by this type of deviation.

The preceding results obtained suggest that the shape of the hysteresis loop does not have a significant effect on the wing-rock properties. To a first approximation, the steady-state wing-rock amplitude in the presence of static rolling-moment hysteresis with sideslip is found to be proportional to the square root of the area of the hysteresis loop. Similarly, although the phase corrections vary according to the geometric shape of the hysteresis loops, their values are relatively small and the main contributor to the wing-rock frequency is still the effective dihedral.

VII. Energy Considerations

The manifestation of wing rock in the limit-cycle type of motion implies that there is no net inflow or outflow of energy into or out of the system when the steady-state motion has been reached. For the single-degree-of-freedom roll motion considered, the work W done to the system in one cycle of motion is given by

$$W = \oint L(\phi, \dot{\phi})\,\mathrm{d}\phi \tag{41}$$

which can also be written as

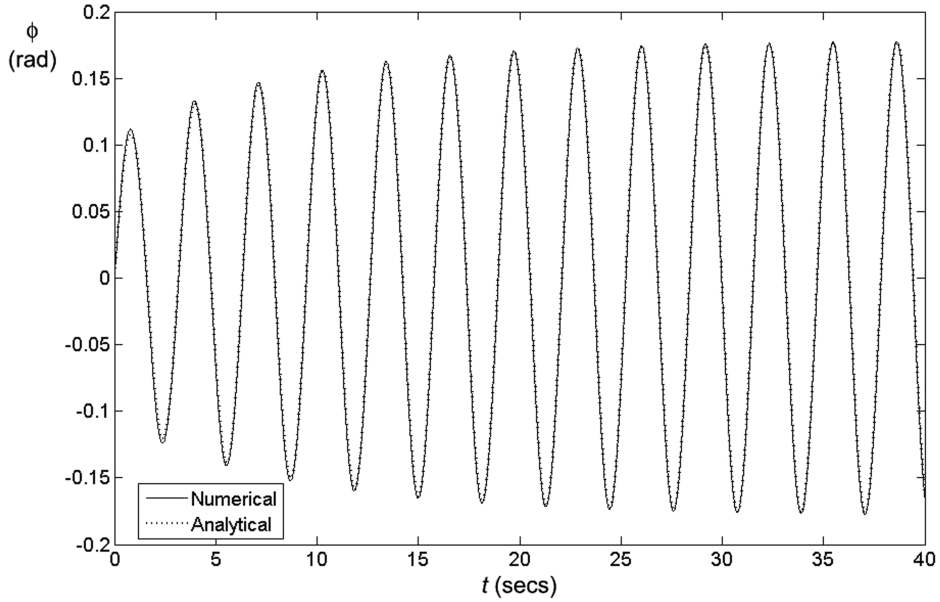

Fig. 10 Wing rock for $C_l - \beta$ hysteresis with gradient deviation; $\omega = 2$ rad $\cdot$ s^{-2}, $\tilde{\mu} = -0.1$ s^{-1}, $\tilde{d} = 0.1$ s^{-2}, and $\Phi = 0.05$ rad, with initial condition $(\phi, \dot{\phi}) = (0, 0.2$ rad/s).

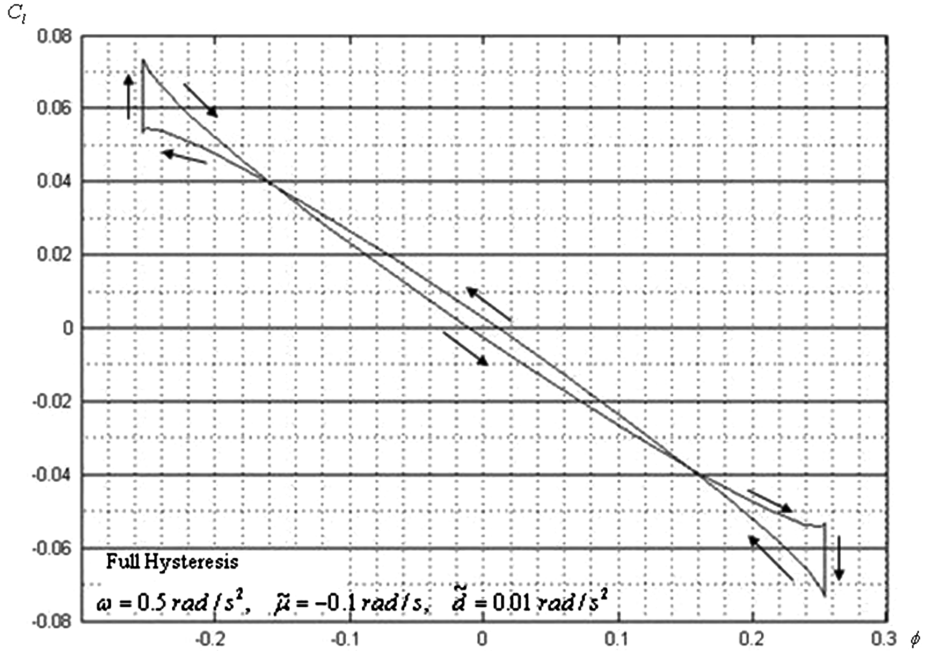

Fig. 11 Steady-state C_l-vs-ϕ response for the full-hysteresis case.

$$w = \oint \left(-\omega_0^2 \phi + \tilde{\mu}\,\dot{\phi} + \tilde{h}(\phi, \dot{\phi}) \right) \mathrm{d}\phi \tag{42}$$

where $w \equiv W/I_{xx}$. It can be shown mathematically that for the various forms of $\tilde{h}$ considered, Eq. (42) does evaluate to zero in the steady-state condition, which is consistent with the previous statement.

Graphically, it means that in steady state, the areas enclosed within the clockwise (destabilizing) and counterclockwise (stabilizing) loops in the C_l-vs-ϕ response curve are identical. Figure 11 depicts the C_l-vs-ϕ curve for the full-hysteresis case, and Fig. 12 shows the C_l-vs-ϕ curve for the partial-hysteresis case. Although the areas enclosed by the counterclockwise and clockwise loops can be shown to be the same for each figure, the pattern of the C_l-vs-ϕ diagrams for the two cases are different in terms of the location of the vertical jumps and the stabilizing/destabilizing loops. The location of the jumps in the C_l-vs-ϕ diagrams corresponds to the location of the jumps in the static rolling-moment hysteresis curves (Figs. 3 and 5). In the full-hysteresis case (Fig. 11), the jumps occur at the amplitudes of the limit cycles, whereas for the partial-hysteresis case (Fig. 12), the jumps occur below the amplitudes. The location of the stabilizing/destabilizing loops is also different for the two examples. In the full-hysteresis case, the stabilizing loop (counterclockwise) appears at the lower values of ϕ, whereas the destabilizing loops appear at the larger values of ϕ. The situation is somewhat reversed in the partial-hysteresis case, in which the stabilizing loops appear at the larger values of ϕ and the destabilizing loop appears at the lower values of ϕ. This suggests the difference of the nature of the flow dynamics for the two cases.

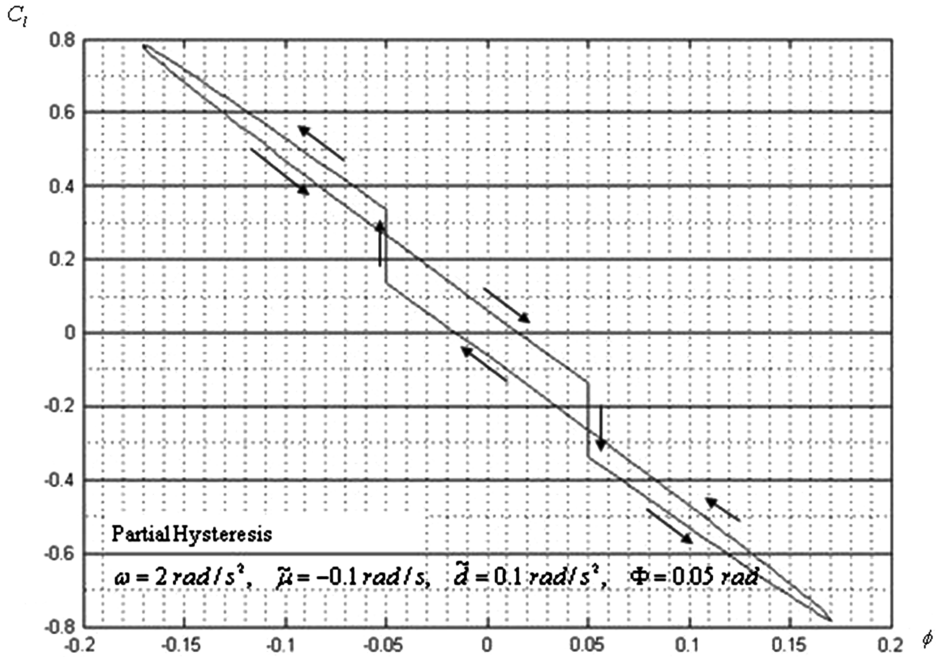

Fig. 12 Steady-state C_l-vs-ϕ response for the partial-hysteresis case.

VIII. Conclusions

Single-degree-of-freedom wing rock due to static rolling-moment hysteresis with sideslip is analyzed in this work using an analytical approach employing the multiple-time-scales method. Approximate solutions relating the hysteresis parameters with the resulting wing-rock properties are obtained, leading to a better understanding on the effects of these parameters to the wing-rock motion. Full and partial-hysteresis cases are considered, as well as the effects of some deviations to the ideal hysteresis curves. The analytical solutions obtained are shown to have a very good agreement with the numerical integration results. Overall, the results suggest that for wing rock due to the static rolling-moment hysteresis with sideslip, the amplitude is proportional to the square root of the static hysteresis loop area, and the frequency is affected mainly by the effective dihedral.

Wing-rock occurrence due to nonhysteretic type of nonlinearity has been associated with the loss of dynamic damping derivatives at high-angle-of-attack flight. The results presented here, however, indicate that when static rolling-moment hysteresis with sideslip is present, wing rock can occur even before the dynamic roll-damping derivative is lost. This suggests that the general onset of wing rock may need to be defined properly in light of the types of nonlinearities present in the system.

References

[1] Nguyen, L. T., Yip, L., and Chambers, J. R., "Self-Induced Wing Rock of Slender Delta Wings," AIAA Paper 81-1883, 1981.

[2] Hsu, C. H., and Lan, C. E., "Theory of Wing Rock," *Journal of Aircraft*, Vol. 22, No. 10, 1985, pp. 920–924.

[3] Konstadinopoulos, P., Mook, D. T., and Nayfeh, A. H., "Subsonic Wing Rock of Slender Delta Wings," *Journal of Aircraft*, Vol. 22, No. 3, 1985, pp. 223–228.

[4] Elzebda, J. M., Nayfeh, A. H., and Mook, D. T., "Development of an Analytical Model of Wing Rock for Slender Delta Wings," *Journal of Aircraft*, Vol. 26, No. 8, 1989, pp. 737–743.

[5] Nayfeh, A. H., Elzebda, J. M., and Mook, D. T., "Analytical Study of the Subsonic Wing-Rock Phenomenon for Slender Delta Wings," *Journal of Aircraft*, Vol. 26, No. 9, 1989, pp. 805–809.

[6] Go, T. H., and Ramnath, R. V., "An Analytical Approach to the Aircraft Wing Rock Dynamics," AIAA Paper 2001-4426, 2001.

[7] Go, T. H., and Ramnath, R. V., "Analysis of the Two Degree-of-Freedom Wing Rock on Advanced Aircraft," *Journal of Guidance, Control, and Dynamics*, Vol. 25, No. 2, Mar.–Apr. 2002, pp. 324–333.

[8] Go, T. H., and Ramnath, R. V., "An Analytical Theory of Three Degree-of-Freedom Aircraft Wing Rock," *Journal of Guidance, Control, and Dynamics*, Vol. 27, No. 4, 2004, pp. 657–664.

[9] Orlik-Rüeckemann, K. J., "Aerodynamics Aspects of Aircraft Dynamics at High Angles of Attack," *Journal of Aircraft*, Vol. 20, No. 9, Sept. 1983, pp. 737–752.

[10] Katz, J., and Levin, D., "Static Measurements of Slender Delta Wing Rolling Moment Hysteresis," *Journal of Aircraft*, Vol. 28, No. 4, Vol. 28, No. 4, 1991, pp. 282–283.

[11] Schmidt, L. V., "Wing Rock due to Aerodynamics Hysteresis," *Journal of Aircraft*, Vol. 16, No. 3, Mar. 1979.

[12] Schiff, L. B., and Tobak, M., "Some Applications of Aerodynamic Formulations to Problems in Aircraft Dynamics," *Dynamic Stability Parameters*, AGARD LS-114, Neuilly-sur-Seine, France 1981, pp. 16.1–16.15.

[13] Ramnath, R. V., and Sandri, G., "A Generalized Multiple Scales Approach to a Class of Linear Differential Equations," *Journal of Mathematical Analysis and Applications*, Vol. 28, Nov. 1969, pp. 339–364.
doi:10.1016/0022-247X(69)90034-1

[14] Ramnath, R. V., Hedrick, J. K., and Paynter, H. M. (eds.), *Nonlinear Systems Analysis and Synthesis*, Vol. 2, American Society of Mechanical Engineers, New York, 1981, pp. 3–54.

[15] Kreyzig, E., "Advanced Engineering Mathematics," 9th ed., Wiley, New York, 2006, pp. 478–534.